Study of Scintillation Crystal Array Parameters for an Advanced PET Scanner Dedicated to Breast Cancer Imaging

A. Vandenbroucke, C.S. Levin

***Abstract*—We present measurements and simulation to determine the optimal crystal array parameters for an advanced PET scanner dedicated to breast imaging. We compared LSO versus LYSO arrays, measured different crystal sizes and various surface finishes and array configurations. We conclude that an 8×8 array of $1 \times 1 \times 1$ mm^3 LYSO crystals with a specular (VM2000) foil on all sides of each individual crystal except the diffuse exit window gives the optimal results for our configuration.**

***Index Terms*—PET, PSAPD, scintillation, LSO, LYSO**

I. Introduction

A PET scanner dedicated to breast cancer imaging is currently under development in our laboratory. The scanner will be built out of scintillation crystal arrays, each coupled to a Position Sensitive Avalanche Photodiode (PSAPD) [1]. With these devices, positioning information is obtained by reading out the four corners of a resistive sheet coupled to the n^+ side of the APD and combining these signals using Anger-type logic. Each module will have 2 scintillation crystal arrays coupled to one PSAPD each. More information about the system can be found in references [2], [3], [4].

This paper reports on the measurements and simulations performed to determine the ideal crystal array configuration. Criteria are energy and time resolution, and crystal identification capabilities.

II. Materials and Methods

A. Experimental setup overview

We used a flex-mounted position sensitive avalanche photodiode (PSAPD) and connected it to a charge sensitive preamplifier (Cremat). The crystal was attached to the PSAPD using optical grease (Bicron BC-630). A ^{22}Na point source provided the annihilation radiation. Timing information was obtained by using a $2 \times 2 \times 2$ cm^3 LSO block connected to a PMT, and detecting radiation in coincidence with the LSO-PSAPD flex. This setup allowed us to change the crystal array while keeping other conditions fixed. A photograph of the setup is shown in Fig. 1.

Pulses were further shaped using NIM electronics, which also formed the triggering logic. Digitization was done using a National Instruments ADC. A schematic of the readout is depicted in Fig. 2.

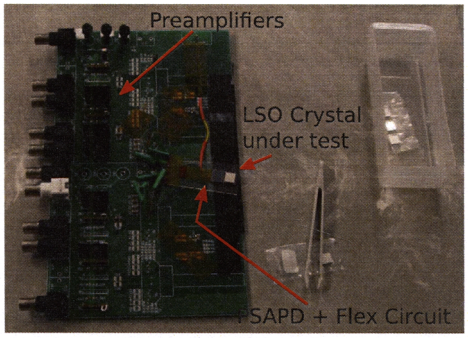

Fig. 1. Photograph showing part of the experimental setup. Only the crystal arrays were changed during the measurements. On the right is a tray filled with crystals to be tested.

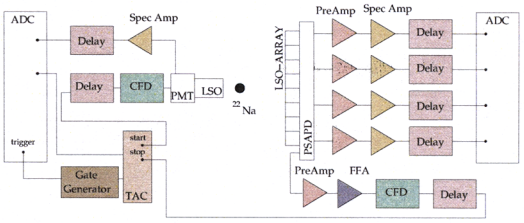

Fig. 2. Schematic of the experimental setup used for the measurements

All arrays used were assembled by Agile Engineering. The following items were investigated:

1) The scintillator material:
   We investigated whether LSO or LYSO yielded the best results for a 4×8 arrays of $1 \times 1 \times 2$ mm^3 crystals.
2) The array configuration:
   4×8 arrays of $1 \times 1 \times 2$ mm^3 LSO crystals were compared to an 8×8 arrays of $1 \times 1 \times 1$ mm^3 LSO crystals.
3) Reflectors and surface treatments:
   Crystals with and without intercrystal reflectors were investigated, as well as crystals with various surface finishes.

In order to investigate systematic effects, all individual crystal peak positions in the flood histogram were sorted geo-

Manuscript received November 14, 2008. This work was supported by NIH grants R01 CA119056 and R33 EB003283. A. Vandenbroucke was supported by a fellowship of the Belgian-American Educational Foundation.

A. Vandenbroucke and C.S. Levin are at the Department of Radiology, Stanford University and associated with the Molecular Imaging Program at Stanford.

metrically so that crystal 1, crystal 8, crystal 57 and crystal 64 correspond to the four corners of the array, as shown in Fig. 3. The data was then sorted according to the geometrical position. Energy spectra for every individual crystal were accordingly obtained. Next, these energy spectra were fit, and finally the Time-to-Amplitude Convertor (TAC) and positioning histograms were filled with photopeak events only.

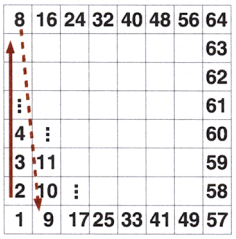

Fig. 3. Crystal numbering schematic

Crystal identification performance was evaluated by using the following Figure of Merit (FOM) calculation:

$$\text{FOM} = \frac{\text{Average distance between the peaks}}{\text{width of the peaks}}$$

This expression has the advantage that it is independent of binning effects, as opposed to the more commonly used peak-to-valley ratio.

B. Simulation

In order to validate some of the experimental results, a Monte Carlo simulation was set up. The simulation uses both GATE [5] and DETECT2000 [6] in the following way: interactions of the 511 keV photon with an LSO sheet is simulated by GATE and stored in a Look-Up Table (LUT). Creation and propagation of optical light is simulated by DETECT2000. This configuration has the advantage that only the crystal array configuration is modified. The various steps in the simulation are schematically shown in Fig. 4.

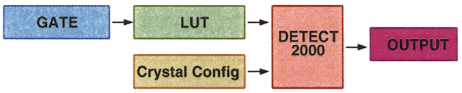

Fig. 4. Schematic of the simulation steps.

III. Experimental Results

A. LSO versus LYSO

Results of the comparison between LSO and LYSO are depicted in Fig. 5. 5 arrays of each were tested. The average time resolution was 4.9 ± 0.3 ns (LSO) versus 4.0 ± 0.3 ns (LYSO), and the average energy resolution $14.8 \pm 0.6\%$ (LSO) versus $13.6 \pm 0.6\%$ (LYSO). No significant differences can be seen for the crystal identification capabilities. This data shows that the LYSO arrays perform better in our configuration. Timing is not corrected for the finite PMT response time.

B. 64 versus 32 crystal arrays

Fig. 6 shows the flood histograms for a 64 crystal array of $1 \times 1 \times 1$ mm^3 crystals and a 32 crystal array of $1 \times 1 \times 2$ mm^3 so that the outer dimensions of both arrays are similar. While

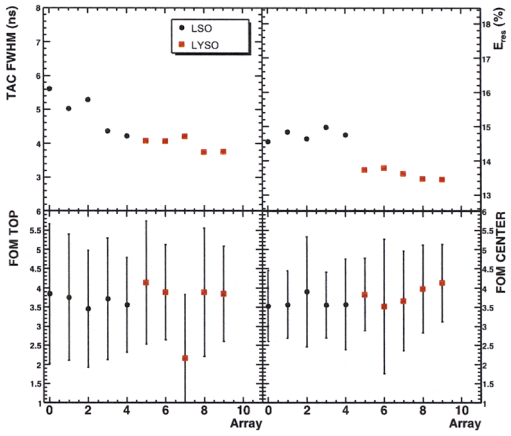

Fig. 5. Upper left (right) shows the timing (% energy) resolution at FWHM for LSO (black circles) and LYSO (red squares) crystal arrays. The left (right) lower panel shows the crystal separation FOM for the top (center) row of the flood histogram.

it is easier to identify 32 crystals, the pincushion distortion caused by the PSAPD's resistive sheet has a larger effect on the larger crystals. It is evident from the image on the right that the individual crystal shapes change across the array: from point-like, over rectangular to banana shaped. These shapes make crystal identification and position binning more difficult. Since the individual crystals show up as dots in the 64 crystal arrays, and since all crystals still are clearly separable, a 64 crystal array is beneficial.

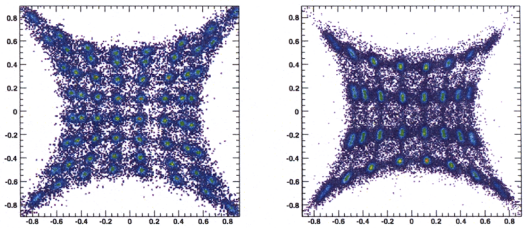

Fig. 6. Flood histogram for an 8×8 array of $1 \times 1 \times 1$ mm^3 crystals (left) and a 4×8 array $1 \times 1 \times 2$ mm^3 crystals (right).

The photopeak position and energy resolution of 6 8×8 and 5 8×4 arrays are compared in Fig. 7. The 8×8 arrays show a systematically higher photopeak position and a slightly better energy resolution ($14.2 \pm 0.8\%$ versus $14.8 \pm 0.6\%$). Also the timing resolution was determined to be better (3.1 ± 0.2 ns versus 4.8 ± 0.3 ns). The timing resolution difference can be explained by taking the resistive sheet coupled to the APD into account. Every spot on the resistive sheet has a different RC-timeconstant. A larger area on the PSAPD's surface thus has a more blurred average RC value. This blurring worsens the time resolution.

These results favor a smaller crystal size. In addition, the

smaller crystal size is advantageous to obtain a finer image resolution.

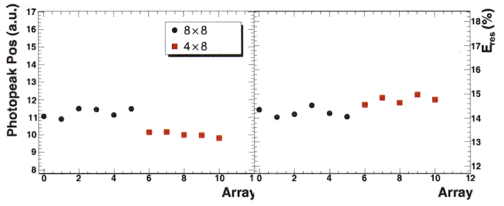

Fig. 7. Left (right) panel compares the photopeak position (energy resolution) of 8×8 arrays of $1 \times 1 \times 1$ mm^3 crystals (black circles) with those of 8×4 arrays of $1 \times 1 \times 2$ mm^3 (red squares) for 6 and 5 crystal arrays respectively.

C. Array configuration

Table I gives an overview of the different crystal configurations used in these tests. Surfaces are either diffuse or polished. The reflector attached to the top side of the array is either VM2000 (made by 3M), or LUMIRROR (made by TORAY). Models C and E have a reflector between individual crystals. Models $A' \cdots E'$ are basically the same as their counterparts $A \cdots E$, except for the exit window being diffuse.

For polished surfaces no total internal reflection occurs for angles smaller than the critical angle $\theta_c = \arcsin \frac{n1}{n2}$, whereas diffuse surfaces are seen as a collection of facets, so reflections occur with angles smaller than the critical angle.

The difference between VM2000 and LUMIRROR is that the former is a specular reflector and the latter a Lambertian (or often referred to as diffuse). For specular reflectors, the reflected angle is the same as the incident angle, $\theta_i = \theta_r$. For Lambertian reflectors on the other hand, θ_r has an intensity profile following Lambert's Law: $\frac{dI(\psi)}{dI_0} = cos\psi$. The thickness of the reflector foils used is 63 μm. Since the outer array dimensions are all similar to match the sensitive area of the PSAPD, crystal arrays without intercrystal reflector have slightly more sensitive area due to larger individual crystal sizes in the array.

Fig. 8 shows no pronounced differences between models *A,B* and *D*, nor between models *C* and *E* respectively. The largest differences are seen between the configurations with and without intercrystal reflector in terms of photopeak position and width. The RMS of the photopeak position across the array is larger for the arrays with an intercrystal reflector. The energy resolution is better for the models without intercrystal reflector: $14.2 \pm 0.8\%$ (C) versus $13.0 \pm 0.5\%$ (B). More light is obtained for 511 keV photoelectric events for the configuration *B* in comparison with model *A*. However, the FWHM is also larger for the former model, yielding a comparable energy resolution.

The arrival time and time resolution are depicted in Fig. 9. The arrival time seems to be longer for the models with an intercrystal reflector foil as opposed to the other models. The time resolution is better for the arrays without intercrystal reflector 3.1 ± 0.2 ns (C) versus 2.6 ± 0.1 (B) ns. Crystal identification is better for the arrays with an intercrystal

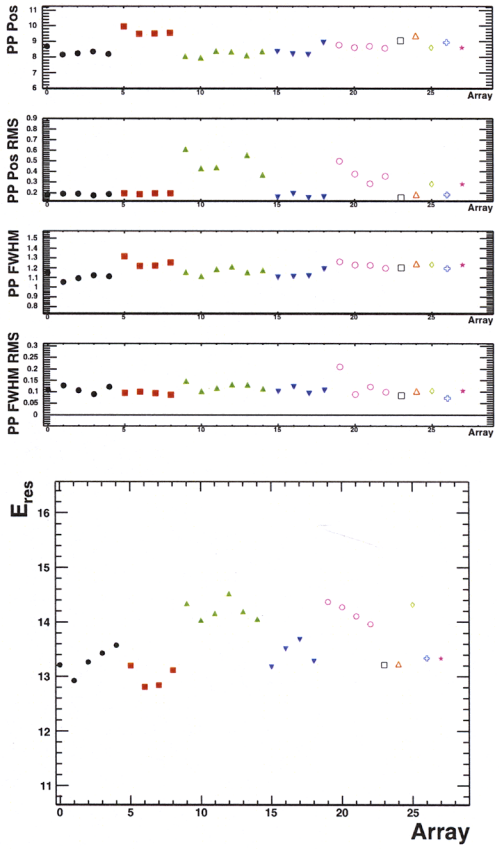

Fig. 8. Top to bottom: average photopeak position, photopeak RMS across the array, average photopeak FWHM and its RMS across the array, and finally the average % energy resolution for models $A, B, C, D, E, A', B', C', D', E'$ from Table I respectively.

reflector as seen from the FOM. Again, no correction for the finite PMT timing was applied.

The roughness of the exit window does not seem to have a significant influence. The same differences between arrays with intercrystal reflector and arrays without intercrystal reflectors are seen as in the case of polished exit windows. However, since only one array for each of the configurations was measured, the statistical significance of the result is limited.

IV. SIMULATION RESULTS

A. Intercrystal reflector simulation

Simulation of the arrays with intercrystal reflectors were implemented by setting the crystal's side finish to 'metal' with a reflection coefficient of 98 %. This assumes that the surface is smooth and covered with a metalized coating representing a specular reflector. Transmission is not considered and a random sampling determines whether the photon is absorbed [6].

The arrays without intercrystal reflector between individual crystals were simulated by implementing a 'polished' surface.

	A	B	C	D	E	A'	B'	C'	D'	E'
Top Reflector	VM2000	VM2000	VM2000	Lumirror	Lumirror	VM2000	VM2000	VM2000	Lumirror	Lumirror
Top Surface	Polished	Diffuse	Diffuse	Polished	Diffuse	Polished	Diffuse	Diffuse	Polished	Diffuse
Bottom Surface	Polished	Polished	Polished	Polished	Polished	Diffuse	Diffuse	Diffuse	Diffuse	Diffuse
Side Surface	Polished	Diffuse	Polished	Polished	Polished	Polished	Diffuse	Polished	Polished	Polished
Sides Reflector	No Reflector	No Reflector	VM2000	No Reflector	VM2000	No Reflector	No Reflector	VM2000	No Reflector	VM2000
# of Crystals	5	4	6	4	4	1	1	1	1	1

TABLE I
TABLE SUMMARIZING THE DIFFERENT CRYSTAL ARRAY CONFIGURATIONS USED IN THE SETUP.

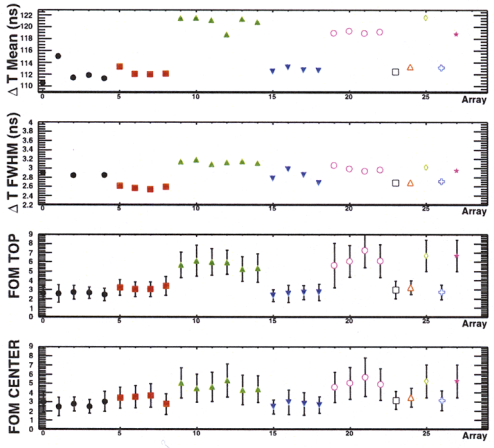

Fig. 9. Top to bottom: average arrival time, average time resolution, FOM for a top and a center row for models $A, B, C, D, E, A', B', C', D', E'$ from Table I respectively.

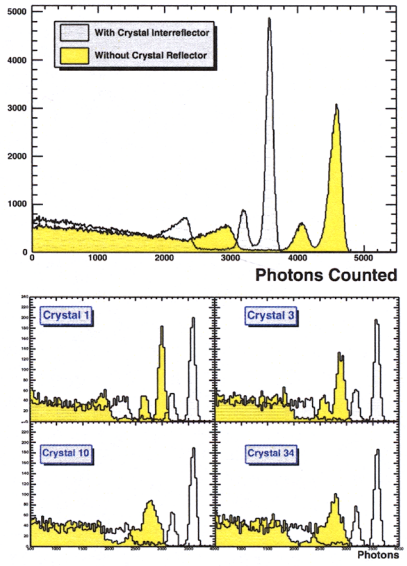

Fig. 10. Top shows the number of photons counted across the entire array per event for arrays with (grey) and without (yellow) intercrystal reflector. The bottom figure shows the same spectra for 4 individual crystals positioned across the array.

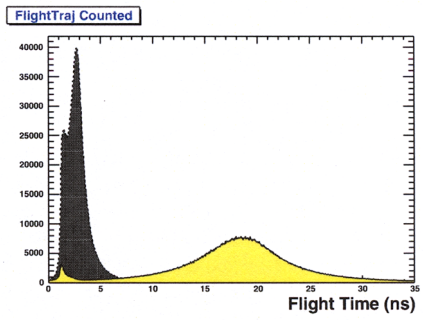

Fig. 11. Flight time of all optical photons in all events for cases with (black) and without (yellow) intercrystal reflectors.

A polished surface is assumed to be flat and in contact with another material, the epoxy glue in our case.

Summing the number of photons in all 64 crystals, the spectrum shown in Fig. 10 is obtained. The photopeak, X-Ray escape peak and Compton edge are clearly visible in both cases. It seems that when having no intercrystal reflector, more light is detected. However, looking at individual crystal spectra, depicted in the lower panel of Fig. 10, we see that the intercrystal reflector arrays give more consistent results across the array, and a better energy resolution. Moreover, in the case of no reflective foils, the energy resolution worsens towards the center of the array.

This observation confirms that in the case of no intercrystal reflector light is shared among many crystals in the array. The latter is also reflected in a completely different arrival time distribution between both cases as shown in Fig. 11. However, the photons with a longer flight time may be of no influence to the signal created by the PSAPD depending on the integration and differentiation time of the readout electronics. Fig. 12 shows the number of photons counted together with the number of photons absorbed for arrays with (black) and without (yellow) intercrystal reflector. If an intercrystal reflector is present, some optical photons get absorbed in the reflective foil.

These results do not match the data presented in section III-C. This discrepancy could be due to a number of reasons. One example could be the shape of the individual crystals not being perfectly rectangular, thus causing different scattering angles. Another reason could be the lack of simulation of the readout electronics, in terms of noise and signal shaping. A less than optimal simulation of the

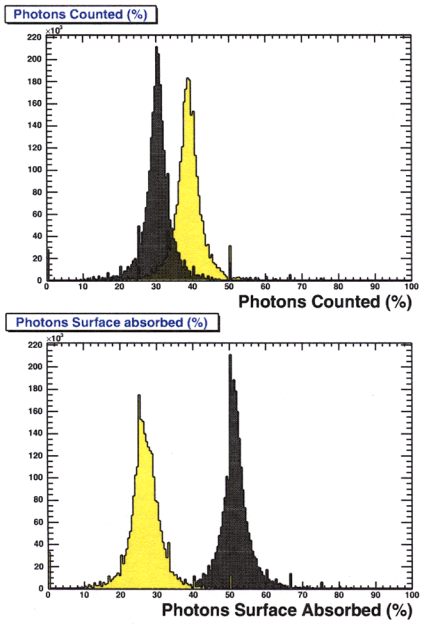

Fig. 12. Number of photons counted and surface absorbed for cases with (black) and without (yellow) intercrystal reflectors.

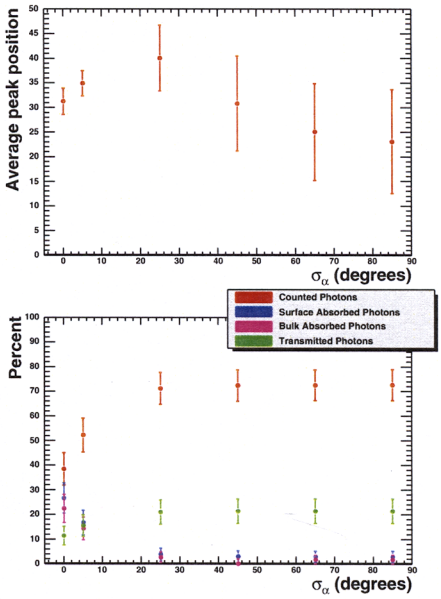

Fig. 13. The upper panel shows the average photopeak position across the array, the error bars being an indication of the deviation across the array. The lower panel shows the number of counted photons together with where the non-counted photons get lost.

crystal surfaces is another possible cause. The latter could be investigated by implementing a more complex reflection pattern than just a specular reflector. Also in the case of arrays with an intercrystal reflector, the simulation may not be fully adequate. Indeed, the simulation assumes full absorbtion in the case of 'metallic' surfaces, while some light may be transmitted.

B. Side surface roughness

In an attempt to explain the differences between model *A* and *B*, the surface roughness of the 4 sides of the crystals were changed. Rough surfaces are assumed to be built of many small surfaces. These surfaces are inclined with a particular angle α with respect to the crystal surface. A combination of these angles yields a Gaussian distribution with mean 0 and standard deviation σ_α.

Fig. 13 shows the position of the photopeak as a function of σ_α. The error bars indicate the RMS of the photopeak position across the array. The distribution seems to be optimal for slightly diffuse crystals. The same figure also shows that more photons are counted for a rougher surface.

While it is experimentally hard to determine the crystal roughness, this result seems to confirm the trend observed in Fig. 8, showing that the diffuse crystals (red squares) have a higher light yield than the polished crystals (black circles). Moreover, the simulations show that an ideal surface roughness can be obtained, evident from Fig. 13.

Fig. 14 shows the different photopeak position across the array for a particular surface roughness with $\sigma_\alpha = 25°$, in an attempt to explain the increasing error bars in Fig. 13. A large

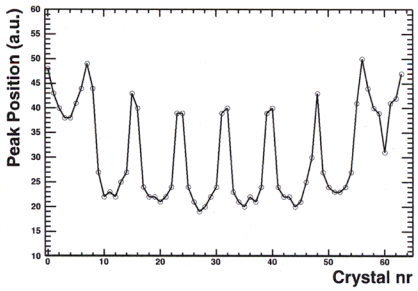

Fig. 14. Photopeak position variation across the array for $\sigma_\alpha = 25°$.

variation in photopeak position as a function of array position can be seen. For increasing angles, larger differences can be seen between crystals on the edge and those in the center, yielding larger error bars in Fig. 13.

C. Exit window roughness

The influence of the surface roughness of the exit face was estimated for the case of an array with intercrystal reflector. No dependence can be seen. This result was confirmed experimentally (not shown here).

According to the manufacturer, arrays with diffuse exit faces are produced more cost-effectively. The lack of exit window roughness dependence in terms of the number of photons counted was convincing to use crystals with a diffuse end in the final configuration.

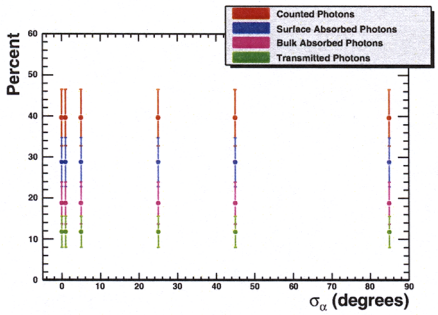

Fig. 15. The number of counted photons together with where the non-counted photons get lost as a function of exit surface roughness.

V. Summary and Conclusion

Our measurements show that an LYSO array performs better than an LSO array in terms of energy and time resolution and for our detector configuration. Additionally, we demonstrated that 8×8 crystal arrays yield better results than 4×8 arrays. The energy and time resolutions for these configurations are given in Table II.

	4 × 8 LSO	**4 × 8 LYSO**	**8 × 8 LSO**
$E_{res}(\%)$	14.8 ± 0.6	13.6 ± 0.6	14.2 ± 0.8
$t_{res}(ns)$	4.9 ± 0.3	4.0 ± 0.3	3.1 ± 0.2

TABLE II
TABLE SUMMARIZING THE % ENERGY RESOLUTION AND THE TIME RESOLUTION AT FWHM FOR DIFFERENT CRYSTAL CONFIGURATIONS.

In terms of crystal configurations, it was shown that arrays without intercrystal reflector have about 10 % better energy and time resolution than those with intercrystal reflector. Having an intercrystal reflector improves the crystal identification, especially at the edges of the array.

Simulations show that photons spread across the array in configurations without intercrystal reflector. This spread causes a longer arrival time for some of the photons. The discrepancy between the simulation and the presented data in terms of crystal array configuration is currently under study.

Experimental observations as well as Monte Carlo simulations suggest it may be possible to optimize the crystal roughness in absence of an intercrystal reflector.

Based on the observations presented in this work, an 8×8 array of $1 \times 1 \times 1$ mm^3 LYSO crystals with intercrystal reflector, polished sides and diffuse entrance and exit windows was chosen.

References

[1] K. Shah, "A novel position sensitive detector for nuclear radiation," RMD, Inc, Watertown, MA, Final Report to the Department of Energy, 2006.
[2] J. Zhang *et al.*, "Performance characterization of a novel thin position-sensitive avalanche photodiode for 1 mm resolution positron emission tomography," *IEEE Trans. Nucl. Sci.*, vol. 54, p. 415, 2007.
[3] A. Vandenbroucke *et al.*, "Performance characterization of a new high resolution PET scinitllation detector," in *Proc. IEEE NSS-MIC*, 2008, in press.
[4] F. Lau *et al.*, "A 1 mm^3 resolution breast dedicated PET system," in *Proc. IEEE NSS-MIC*, 2008, in press.
[5] S. Jan *et al.*, "GATE: a simulation toolkit for PET and SPECT," *Phys. Med. Biol.*, vol. 49, pp. 4543–4561, 2004.
[6] C. Moisan *et al.*, *DETECT2000, The Object Oriented C++ Language Version of Detect*, Laval University, Quebec City, Quebec, Canada, 2000, version 5.0.